
Article:
Gidalevitz, T., Biswas, C., Ding, H. et al. (2004) Identification of the N-terminal Peptide Binding Site of Glucose-regulated Protein 94. Journal of Biological Chemistry, 279 (16). pp. 16543-16552. ISSN: 1083-351X

https://doi.org/10.1074/jbc.M313060200

THE JOURNAL OF BIOLOGICAL CHEMISTRY Vol. 279, No. 16, Issue of April 16, pp. 16543–16552, 2004
Printed in U.S.A.

Identification of the N-terminal Peptide Binding Site of Glucose-regulated Protein 94*

Received for publication, December 1, 2003, and in revised form, January 28, 2004
Published, JBC Papers in Press, January 30, 2004, DOI 10.1074/jbc.M313060200

Tali Gidalevitz,[a,b,c,d,e] Chhanda Biswas,[a,b,d] Hua Ding,[b] Dina Schneidman-Duhovny,[f] Haim J. Wolfson,[f] Fred Stevens,[g] Sheena Radford,[c,h] and Yair Argon[a,b,i]

From the [a]Department of Pathology, the University of Chicago, Chicago, Illinois 60637, [b]The Children's Hospital of Philadelphia, The University of Pennsylvania, Philadelphia, Pennsylvania 19104, the [f]School of Computer Science, Raymond and Beverly Sackler Faculty of Exact Sciences, Tel Aviv University, Ramat Aviv, 69978, Israel, the [g]Argonne National Lab, Argonne, Illinois 60439, and the [c]School of Biochemistry and Molecular Biology, University of Leeds, Leeds LS2 9JT, United Kingdom

Because the stress protein GRP94 can augment presentation of peptides to T cells, it is important to define how it, as well as all other HSP90 family members, binds peptides. Having previously shown that the N-terminal half of GRP94 can account for the peptide binding activity of the full-length protein, we now locate this binding site by testing predictions of a molecular docking model. The best predicted site was on the opposite face of the β sheet from the pan-HSP90 radicicol-binding pocket, in close proximity to a deep hydrophobic pocket. The peptide and radicicol-binding sites are distinct, as shown by the ability of a radicicol-refractive mutant to bind peptide. When the fluorophore acrylodan is attached to Cys[117] within the hydrophobic pocket, its fluorescence is reduced upon peptide binding, consistent with proximity of the two ligands. Substitution of His[125], which contacts the bound peptide, compromises peptide-binding activity. We conclude that peptide binds to the concave face of the β sheet of the N-terminal domain, where binding is regulated during the action cycle of the chaperone.

Glucose-regulated protein 94 (GRP94),[1] also known as gp96, is a member of the HSP90 family of molecular chaperones and can dramatically stimulate T cell responses by two mechanisms: enhancement of peptide presentation to the adaptive arm of the immune system (1) and stimulation of innate immunity (2). Because of these activities, tumor-derived GRP94 can be used to elicit immune response against the tumor and is potentially a powerful immunotherapeutic tool (3). The antigen-presentation activity was shown not to be due to any mutation in GRP94 that would enhance its immunogenicity, but rather due to its ability to bind peptides (1, 4). The GRP94-peptide complexes are known to be taken up by a subset of antigen-presenting cells via receptor-mediated endocytosis (5), and the chaperoned peptides are then re-presented on endogenous antigen-presenting cells MHC class I molecules on the cell surface. Although peptide binding is a general activity of many molecular chaperones, it has been argued that GRP94 is among the most effective of such chaperones in enhancing antigen presentation.

Despite its importance, the GRP94-peptide interaction and the identity of the peptide-binding site have not been characterized in detail. They are crucial issues toward understanding the immunostimulatory action of GRP94. The mode of peptide binding by GRP94 may also inform about its activity as a chaperone of selected membrane-bound and secreted proteins (6), although the connection between the two activities is yet to be elucidated. The same questions are also unanswered for all other HSP90 chaperones, despite the central role of these cytosolic chaperones in organizing signaling complexes and regulating transcription factor (6). Several peptides derived from vesicular stomatitis virus (VSV) have been shown to bind GRP94. VSV8 is an octamer (RGYVYQGL) from the N protein of VSV and is the dominant T cell epitope of the virus, presented via MHC class I K^b to specific T cells (7). The structure of a complex of this peptide with MHC class I has been solved (8). VSV8 has been eluted from GRP94 purified from a VSV N protein-transfected cell line (9), and the peptide has been shown to bind directly to purified GRP94 *in vitro* (1). Peptide A is a 15-mer (KRQIYTDLEMNRLGK) from the glycoprotein of the virus and is not known to be immunogenic (1, 10, 11). However, this peptide binds GRP94, as do other peptides from the VSV G protein, including LSSLFRPKRRPIYKS (1). Another viral peptide known to bind GRP94 is YVNTNMG from the core protein of hepatitis B virus, which is similar to a known HLA-A11 antigenic peptide (12). The only non-viral peptides rigorously shown to bind GRP94 are the ovalbumin ^{257}SIINFEKL^{264} peptide (13), and a mouse leukemia tumor antigen IPGLPLSL from a mutated *Akt* (14).

No common sequence motif is obvious from comparing these peptides. Spee and Neefjes (15) used radioactive peptides with photo-reactive side chains to explore the peptide preferences of GRP94. No obvious size preference was found, and even 40-mers could bind the chaperone. The only sequence specificity found was that 9-mers with basic or acidic amino acids in positions 2 and 9 bind relatively weakly to GRP94. In two cases, the VSV N-derived and the RBL tumor-derived antigens

* This work was supported in part by National Institutes of Health Grants CA-74182 and AI-30178 (to Y. A.) and DK43757 (to F. S.). Work carried out in the Astbury Centre for Structural Molecular Biology, University of Leeds, was supported by the Biology and Biotechnology Research Council (BBSRC). The costs of publication of this article were defrayed in part by the payment of page charges. This article must therefore be hereby marked "*advertisement*" in accordance with 18 U.S.C. Section 1734 solely to indicate this fact.

[d] Both authors contributed equally to this work.
[e] Supported in part by National Institutes of Health Training Grant HL07237.
[h] A BBSRC Professorial Fellow.
[i] To whom correspondence should be addressed: Division of Cell Pathology, The Children's Hospital of Philadelphia, 3615 Civic Center Blvd., Philadelphia, PA 19104. Tel.: 267-426-5346; Fax: 267-426-5165; E-mail: yargon@mail.med.upenn.edu.

[1] The abbreviations used are: GRP94, glucose-regulated protein 94; HSP90, heat shock protein 90; VSV, vesicular stomatitis virus; MHC, major histocompatibility complex; ANS, 8-anilino-1-naphthalene sulfonic acid; DEPC, diethyl pyrocarbonate; Pipes, 1,4-piperazinediethanesulfonic acid; Ni-NTA, nickel-nitrilotriacetic acid.

(1, 14) not only are the octamer antigenic peptide associated with GRP94, but also their larger precursors. This raises the question of what sequence or structure features are compatible with peptide binding to GRP94.

The limited amount of information about the peptide binding activity of GRP94 is due in part to the low stoichiometry of binding (only about 1% of the protein had been shown to bind peptides (16)) and slow binding kinetics (17). These technical obstacles also hindered the identification of structural determinants of the peptide-binding site and its regulation. We showed that the N-terminal third of GRP94 constituted a peptide-binding entity and demonstrated that peptide binding to this fragment is specific, is inhibited by the pan-HSP90 inhibitors radicicol and geldanamycin, and has a binding stoichiometry close to 1 mole of peptide per mole of GRP94 (17). In addition, our data indicated that the peptide specificity of this site is different from that of another endoplasmic reticulum-resident stress protein, BiP (17). In the present work we use molecular modeling, biochemical characterization, and site-directed mutagenesis to identify a peptide-binding site located within the N-terminal domain, on the face opposite the radicicol-binding site, and show that His^{125} is located in the binding site and is directly involved in the binding activity.

EXPERIMENTAL PROCEDURES

Recombinant Proteins

N1–355—The construct for expression of N1–355 in insect cells and the purification procedure are described previously (17). Recombinant N1–355 contained an N-terminal His_6 tag, followed by the first 355 amino acids of a mature sequence of GRP94 and a C-terminal ER1 targeting signal KDEL.

N34–355—The sequence coding for the first 33 amino acids of N1–355 was deleted by PCR cloning. The resultant PCR product was inserted into the pQEXa vector (Qiagen) using BamH1 and XmaI so as to add a His_6 tag followed by a factor Xa recognition sequence at N terminus. The plasmid was transformed into M15 *Escherichia coli*, which were allowed to grow to mid-log phase and then incubated with 1 mM isopropyl-1-thio-β-D-galactopyranoside for 4 h at 27 °C to induce protein expression. Bacteria were harvested and lysed in 1% Nonidet P-40 (Sigma Chemicals) in 20 mM phosphate buffer, pH 7.2, containing 500 mM NaCl and 20 mM imidazole. N34–355 was purified from the detergent lysates by affinity chromatography on Ni-NTA columns (Qiagen), according to the manufacturer's instructions. Bound proteins were eluted with 500 mM imidazole, dialyzed, and concentrated. The protein was stored in 25 mM HEPES (pH 7.2), 110 mM KOAc, 20 mM NaCl, 1 mM $Mg(OAc)_2$, 0.1 mM $CaCl_2$ (buffer A) containing 10–20% sucrose at −80 °C. When needed, the N-terminal extension containing the His_6 tag was removed by digestion with factor Xa (Novagen) according to the manufacturer's instructions. The reaction mixture was re-purified over a Ni-NTA column, and the flowthrough containing only the cleaved N34–355 was used. The cleaved protein appeared 2–3 kDa smaller on SDS-PAGE compared with the parent protein, consistent with the removal of 17 amino acids (not shown). After digestion, the heptamer PYNGTGS precedes Ala^{34} of the mature N34–355 sequence.

Mutant Proteins—Amino acids substitutions were introduced into the vector encoding N34–355 with the QuikChange kit (Stratagene). Mutations were verified by sequencing and, when appropriate, by restriction enzyme analyses. The proteins were expressed in bacteria and purified as described above.

Peptides

Peptides were synthesized at the University of Chicago facility and verified by mass spectroscopy. The sequences of the two binder peptides were: VSV8, RGYVYQGL, from the VSV N protein; Pep A, KRQIYTDLEMNRLGK, from the VSV G protein. Stock solutions were prepared in water and stored at −80 °C. Peptide concentrations were determined by a BCA assay (Pierce). Where indicated, peptides were iodinated by the IODO-BEADs method (Pierce), and unincorporated iodine was removed by passage over a short Dowex AG 1-X8 column. The specific radioactivity of the peptides was routinely 2×10^{14} to 1×10^{15} cpm/mol.

Peptide Binding Assays

Two types of binding assays were used. The solution binding assay was performed as described previously (17). Briefly, recombinant proteins were incubated with iodinated peptide under saturating conditions, and radioactivity associated with protein-peptide complexes was measured after separation of free peptide over spin columns containing 0.2–0.8 ml of packed P-30 beads (Bio-Rad) in buffer A. Iodinated peptide without protein was used as background control for spin column separation.

A solid-phase binding assay (referred to as plate assay in the text) is described and validated elsewhere.[2] Briefly, 96-well plates (Costar 3590 High Binding, Corning, NY) were coated with peptides prior to assay, and the recombinant proteins in 100 μl of buffer A were allowed to bind for 90 min. Binding was quantified by HRP-rabbit anti-His_6 (Amersham Pharmacia Biotech), and color development was monitored at 415 nm with a BioTek plate reader. Because both N1–355 and N34–355 normally reached saturation at the input level of 0.7 or 1 μg, the A_{415} value at this level was defined as 1, and all data points were normalized to it. Inhibition by 300 μM radicicol (Sigma; stock solution in Me_2SO) was used as a specificity control.

Because peptide binding to GRP94 is saturable and specific, yet the off-rate is exceedingly slow (17), K_a values were estimated graphically from the fractional occupancy curves (A_{415} value at a given protein input relative to A_{415} value at saturation as a function of protein input). When the binding reaction is not in equilibrium, these values are valid as comparative parameters among the various mutants.

Gel Electrophoresis

Analysis of protein conformation by blue native gel electrophoresis was accomplished by using 5–15% gradient acrylamide gels in the Laemmli gel system without SDS (18), with Coomassie Brilliant Blue G-250 (Sigma Chemicals) included in the cathode buffer. Thyroglobulin, ferritin, and bovine serum albumin were used as molecular weight standards.

Protein Modifications

Binding of the fluorescent dye 8-ANS (Molecular Probes, Eugene, OR) to proteins was performed by incubating 5 μM ANS with 0.5 μM of the appropriate N355 construct in 500 μl of buffer A.

For acrylodan (6-acryloyl-2-dimethylaminonaphthalene) modification, recombinant protein (10 μM) was incubated at 4 °C overnight in the presence of 100 μM acrylodan (Molecular Probes) in 50 mM ammonium acetate buffer, pH 6.9, and free acrylodan was removed using a spin column. For the experiments measuring the effect of peptide on N355-acrylodan, peptide was added to the final concentration of 100 μM; equivalent volume of buffer was added to control samples. The mixtures were heat-shocked at 50 °C for 10 min and diluted to 500 μl, and fluorescence measurements were performed on a PTI fluorometer. Samples were excited at 350 nm for ANS and 390 nm for acrylodan, and the emission spectra were collected between 400 and 600 nm. The slit widths were set at 2 nm for excitation and 2–6 nm for emission.

Before modification of histidines with DEPC, wild type, or H125D N34–355 (800 μg each) were treated with 24 units of factor Xa (Novagen) in buffer A overnight at 25 °C and then repurified using Xarex-agarose (Novagen) to remove factor Xa and Ni-NTA-agarose to remove the His_6-containing peptide. The His-cleaved proteins were reacted with peptide A (or solvent alone) at 12 μM protein and 2.8 mM peptide in buffer A overnight at 25 °C. Free peptide was removed, and the buffer was exchanged to 50 mM ammonium acetate, pH 6.8, using P10 spin columns. Both free N34–355 and the protein-peptide complexes were reacted with 1 mM DEPC (Sigma Chemical Co.) at 25 °C or with EtOH as a solvent control. Incubation for 15–20 min gave complete His modification, as determined by monitoring the reaction at 240 nm (19). Where indicated, the carbethoxyhistidine was reverted back to histidine by treatment with 400 mM hydroxylamine for 15 min at 25 °C (20).

Mass Spectrometry

Samples were diluted to 20 μM final concentration in sinapinic acid saturated with acetonitrile and 1% trifluoroacetic acid. 1–2 μl of each sample was adsorbed onto a Ciphergen gold chip and allowed to air dry. Masses were measured by using the surface-enhanced laser desorption ionization/time-of-flight ProteinChip Reader (Ciphergen).

RESULTS

GRP94-bound Peptide Is Contained within a 188-Residue Fragment—Previously we demonstrated that a truncated version of GRP94, containing amino acids 1–355, is sufficient to

[2] C. Biswas, T. Gidalevilz, and Y. Argon, manuscript in preparation.

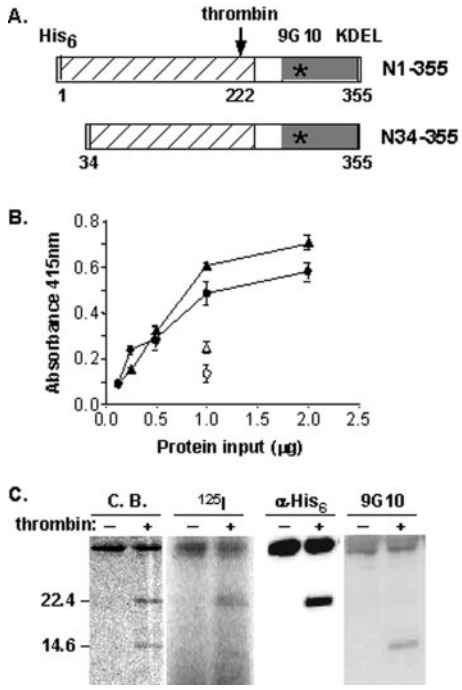

FIG. 1. **A minimal portion of GRP94 is sufficient for peptide binding.** *A*, schematic of recombinant proteins used. N1–355, the protein used in (17), contains the first 355 amino acids of GRP94, starting from the DDEVD N terminus of the mature protein. N34–355 is a version expressed in bacteria, where the first 33 amino acids of mature GRP94 are deleted. *Hatched box*, the N-terminal domain, containing the nucleotide/geldanamycin/radicicol-binding site. *Dark gray box*, an acidic domain needed for at least one of the activities residing in the N-terminal domain. *Light gray box*, His_6 tag. In N34–355 the tag is followed by a factor Xa cleavage site. N1–355 terminates with a KDEL endoplasmic reticulum retrieval signal, which is absent in N34–355. The single thrombin cleavage site after Arg^{222} is marked, as is the region containing the 9G10 monoclonal anti-GRP94 epitope (*). *B*, peptide binding ability of N1–355 and N34–355. The two versions of recombinant chaperone were tested, at the doses indicated, for binding of the 8-mer peptide VSV8 in the 96-well plate assay (see "Experimental Procedures"). *Filled triangles*, N1–355; *filled squares*, N34–355; *empty symbols* show inhibition of peptide binding by radicicol. *C*, thrombin digestion of N1–355-iodinated peptide complex. *C.B.*, Coomassie Blue-stained gel after partial proteolysis with thrombin, showing the cleavage of the recombinant protein into two fragments. ^{125}I, autoradiography of the same gel, showing that the iodinated peptide co-migrates with the larger thrombin fragment. α-His, Western blot for the N-terminal His tag identifying the 22.4-kDa band as the N-terminal fragment. 9G10, Western blot for the epitope residing in the acidic domain identifying the 14.6-kDa band as the C-terminal fragment. The *larger band* at the top of the gels is undigested material.

account for the ability of the full-length protein to bind immunologically relevant peptides, such as the VSV major T cell antigen, VSV8. We also showed that this activity was subject to regulation by the pan-HSP90 inhibitors radicicol and geldanamycin (17). To further locate this peptide-binding site, a shorter version of recombinant GRP94 that lacked the first 33 amino acids of the mature protein (N34–355, Fig. 1*A*) was cloned and over expressed in *E. coli*. This recombinant protein bound VSV8 with a binding curve very similar to that of N1–355 (Fig. 1*B*), showing that the first 33 amino acids are not essential for the peptide-binding activity. To define an even smaller fragment containing the peptide-binding site, we took advantage of the single thrombin site in N34–355, C-terminal to Arg^{222}, and asked whether a complex of N34–355 and peptide remains intact after cleavage with thrombin. Following the digestion, two bands were detectable by Coomassie Blue staining corresponding to the predicted N-terminal 22.4-kDa and C-terminal 14.6-kDa fragments (Fig. 1*C*). The assignment of the fragments was confirmed by antibodies specific to either the N terminus of N34–355 (anti-His_6) or to residues 261–276 near the C terminus (9G10 (21)). Because the GRP94-peptide complex is resistant to SDS (1, 17) peptide-bound protein fragments can be detected after SDS-PAGE by the radioactivity of the bound iodinated peptide. In the absence of thrombin, a radioactive band corresponding to the uncleaved complex was detectable. After partial thrombin digestion, an additional radiolabeled band of apparent molecular mass of 22.4 kDa was detected after SDS-PAGE separation, whereas the other 14.6-kDa fragment was not labeled (Fig. 1*C*). These data suggest, therefore, that amino acids 34–222 of GRP94 are sufficient to retain the bound peptide.

Molecular Modeling of the GRP94-Peptide Complex—We next took advantage of previously published data (22, 23) to create a computer model of potential peptide-binding sites. First, we used the crystal structure of the N-terminal domain of HSP90 (Protein Data Bank files 1YER and 1A4H) to generate an energy minimized, predicted structure of the highly homologous segment of GRP94 (51% identity between yeast HSP82 and mouse GRP94). Second, we used the known structure of the antigenic peptide VSV8, which was determined in association with MHC class I (2MHC (8)). Third, making the simplifying assumption that the conformation of VSV8, when bound to GRP94, is essentially similar to its conformation when bound to MHC class I, we used the docking algorithm PatchDock (24) to predict potential binding sites. The algorithm searches the protein surface for locations with highest geometric shape complementarity to the ligand molecule and docks the ligand into these locations. Such docking solutions usually produce clusters in different protein cavities, because binding in cavities enables greater shape complementarity. In addition, statistical data about atomic contacts of VSV8 with MHC class I was collected and used to score the docking solutions. The highest scoring solutions in terms of shape complementarity and statistical score were selected.

The Peptide-binding Site Is Distinct from the Radicicol-binding Pocket—The seven best solutions mapped to two potential docking sites. One site overlaps with the radicicol-binding pocket (Fig 2*A*), the largest cavity in the protein. This site was considered unlikely, because previous data showed that radicicol and peptide could bind simultaneously. We therefore asked whether mutants that did not bind radicicol could still bind peptides. Relying on the solved structure of the complex between yeast HSP90 N-terminal domain and radicicol (23) and on the similarity between HSP90 and GRP94 (25), we mutated residues Asp^{128} and Gly^{132} simultaneously, to Asn and Ala, respectively. Asp^{93} in HSP90 (corresponding to Asp^{128} in GRP94) makes a crucial hydrogen bond with radicicol, and Gly^{97} packs tightly against the inhibitor and also serves to position helix 4, an important portion of the binding pocket (22, 23, 26). The D93N mutant of HSP90 does not bind ATP (27), so the double mutant of GRP94 was expected to be unable to bind radicicol. Recombinant N34–355 D128N,G132A mutant (RadR) was soluble, mostly monomeric, and expressed the conformation-sensitive epitope for the antibody 9G10, like the wild type protein. To test whether the RadR mutant binds radicicol, we used two functional tests (see Ref. 17 for details): loss of the 9G10 epitope and acquisition of a compact conformation with increased mobility in native blue gels. Both changes have been shown to reflect the conformational change in the protein upon radicicol binding (17). The resultant mutant was refractive to treatment with radicicol, as judged by the continued exposure of the 9G10 epitope (data not shown) and lack of acquisition of a compact conformation (Fig. 3*A*). Despite lack of radicicol binding, the RadR protein bound peptide effectively (Fig. 3*C*), with only a small reduction in the apparent association con-

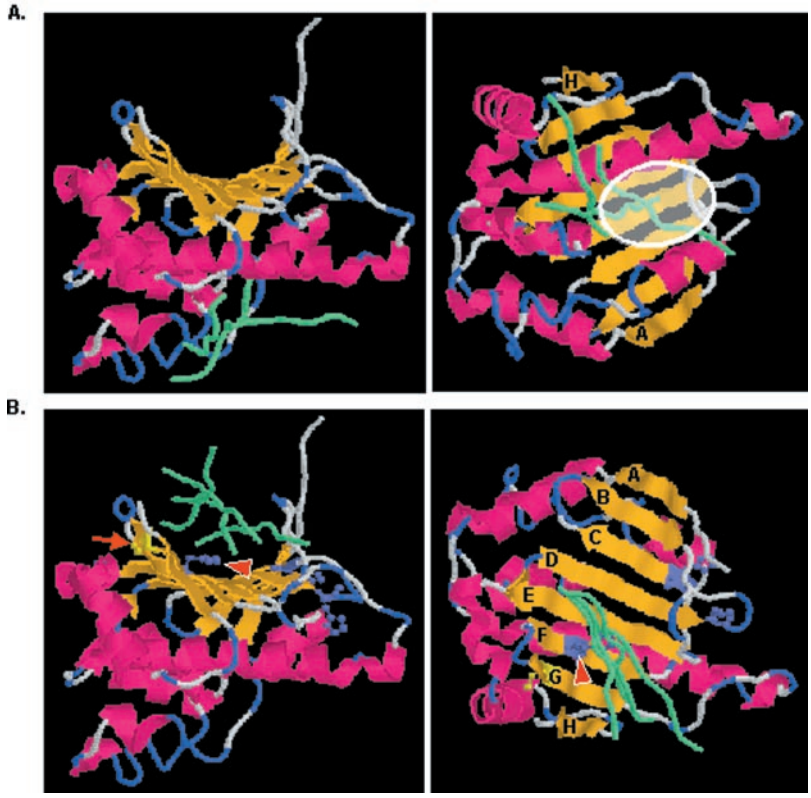

FIG. 2. **Molecular docking model.** The relevant sequence of murine GRP94 (from amino acid 46 to 269) was threaded through the solved structure of the N-terminal domain of yeast HSP90 (PDB file 1YER (26)), using the BioSym software, and energy minimized. The structure of the peptide VSV8 was taken from the solved structure of the complex of VSV8 and MHC class I K^b (8). VSV8 was then docked onto the modeled GRP94 structure using the program PatchDock, assuming that it would bind to GRP94 in the same conformation as to MHC class I. The highest ranking docking solutions are shown. They are divided between two possible sites, shown in *green* in *panels A* and *B*, respectively. *A*, three peptide docking solutions partially overlap with the radicicol/geldanamycin-binding site. *Left panel*, side view from the C-terminal end along the axis of the β sheet. *Right panel*, *bottom view*. *White oval*, outline of the radicicol-binding site. *B*, four docking solutions map over part of the β sheet. *Left panel*, view along the axis of the β sheet, same as in *A*. *Right panel*, *top view*. The sole cysteine and three histidines are shown in *ball-and-stick* representation, in *yellow* and *light blue*, respectively. *Red arrow*, Cys^{117}; *red arrowhead*, His^{125}; *A–H*, strands of the β sheet.

stant compared with the WT protein. Consistent with the lack of radicicol binding, the peptide-binding activity of RadR mutant was not inhibited by pre-treatment with radicicol, whereas the activity of wild type N34–355 was inhibited significantly (Fig. 3*B*). We conclude that not only is the peptide-binding site within N34–355 distinct from the radicicol-binding site (17), but abolition of inhibitor binding does not affect the ability to bind peptides.

Peptide Binding Affects the Environment of the Binding Site for Two Hydrophobic Probes—The other potential peptide docking site is on the opposite side of the β sheet, where there is a large saddle-like surface made of eight β strands. Side barriers to this saddle are provided by two loops, Asp^{170}-Arg^{222} and Lys^{119}-Asn^{122}, plus part of a strand H (Val^{260}-Ser^{263}) that is the end of the modeled sequence (Fig. 2*B*). Four of the highest scoring solutions predicted that VSV8 could fit well within this saddle (Fig. 2*B*). The peptides would fit at an angle of ~70° relative to the long axis of the β sheet across strands E–H, and most of the surface contact would be with the β sheet.

This putative peptide-binding site is in close proximity to a deep hydrophobic pocket (Fig. 4). Hydrophobic residues from strands E, F, G, and H, as well as from the helix and loop leading to the strand H and the long helix are predicted to form this pocket. The edge strand (H) of the β sheet and preceding loop, which form a part of an entrance to this pocket (Fig. 4*B*), have been shown to contribute to the binding site of the hydrophobic dye bis-ANS (28). We therefore speculated that this pocket can accommodate various hydrophobic probes, such as bis-ANS, ANS, acrylodan, and Nile Red, which have been reported to bind to GRP94 (11, 28) (detailed characterization of this hydrophobic pocket is provided elsewhere). The emission spectrum of ANS-labeled N1–355 had a maximum around 474 nm (Fig. 5*A*), as expected if ANS was indeed bound in a hydrophobic environment (29). When ANS-labeled N1–355 was incubated with peptide A, the intensity of ANS fluorescence decreased and its emission maximum was blue-shifted slightly (Fig. 5*A*). Such decreased ANS fluorescence is consistent with peptide A binding affecting, either directly, or via conformational changes, the environment of the fluorophore. Alternatively, if ANS and peptide compete for the same binding site, it may be due to the release of ANS. The latter explanation can be ruled out due to blue shift of ANS emission, so we favor the notion that peptide binds in proximity to the hydrophobic pocket.

If peptide in fact binds as predicted, it should also affect the environment of other hydrophobic probes. Strand G has the sole cysteine residue (Cys^{117}) in N1–355, whose side-chain points into the hydrophobic pocket (Fig. 4), so we modified the protein with the Cys-specific naphthalene derivative acrylodan (11, 30). Although acrylodan has a very low quantum yield in aqueous solutions, its fluorescence is markedly increased upon reaction with thiols (30), and then the fluorescence is highly sensitive to the hydrophobicity of its environment. As shown in Fig. 5*B*, when excited at 390 nm, acrylodan-modified N1–355 had emission maximum around 474 nm, as expected if the fluorophore was in a highly hydrophobic environment. Free acrylodan had a maximum at about 520 nm. Denaturation of the N1–355-acrylodan conjugate with 6 M guanidine hydrochloride abolished the fluorescence at 474 nm and gave rise to the

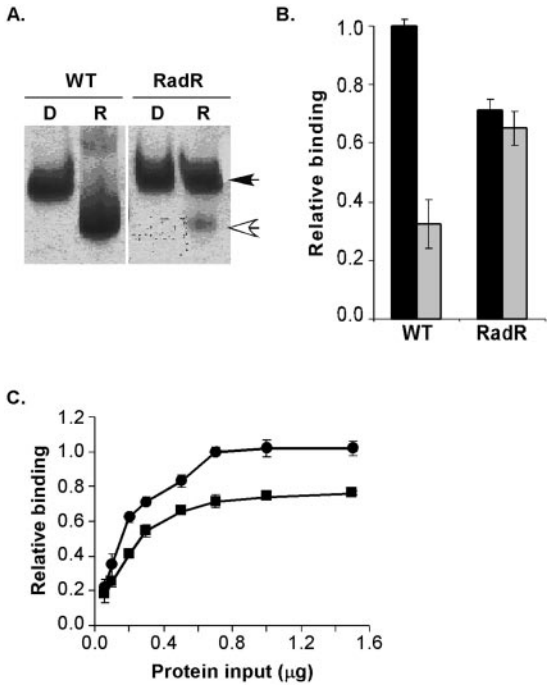

FIG. 3. **The radicicol-refractive mutant N34–355 D128N,G132A still binds peptide.** *A*, D128N, G132A mutant of N34–355 (*RadR*) is refractive to radicicol treatment. N34–355 (*WT*) and RadR proteins were incubated for 15 min with either Me_2SO or radicicol and resolved on a blue native gel. Radicicol-bound WT protein migrates through the gel more rapidly, due to a conformational change in the protein (17). The ability of the RadR protein to bind radicicol is dramatically reduced. *Black arrow*, unmodified protein; *white arrow*, radicicol-bound protein. *B*, peptide binding by RadR mutant is not affected by radicicol and is similar at saturation to that of WT protein. Binding of N34–355 and RadR proteins to VSV8 peptide was measured by the plate assay (see "Experimental Procedures"). *Black bars*, binding in the absence of inhibitor; *gray bars*, binding in the presence of radicicol. Data are averages of triplicate samples. *C*, dose binding of N34–355 and RadR proteins. Binding to VSV8 peptide was measured in a plate assay. *Circles*, WT protein; *squares*, RadR mutant. Data are averages of triplicate samples.

same emission maximum as free acrylodan in 6 M guanidine, indicating that the observed fluorescence is dependent on the tertiary structure of the protein. As expected for the covalent modification, the fluorescence intensity of the denatured N1–355-acrylodan conjugate was significantly higher than that of free acrylodan (Fig. 5*B*). These spectral properties fulfill the expectation that acrylodan is located in a hydrophobic pocket when bound covalently to Cys^{117}. Therefore, acrylodan modification of N1–355 provides a defined fluorescence probe for detection of molecular changes.

To test whether modification with acrylodan affects peptide binding by N1–355, we incubated acrylodan-modified and unmodified proteins with a saturating amount of iodinated VSV8 and measured peptide binding to each. Acrylodan-conjugated protein was capable of binding peptide essentially like the unmodified protein (Fig. 5*C*), showing that acrylodan does not interfere with the binding activity. Importantly, the fluorescence of acrylodan was partly quenched in the presence of peptide (Fig. 5*D*). These data are in good agreement with the model in Fig. 2*B*, which predicts that the peptide-binding site is distinct from but in close proximity to the hydrophobic pocket.

These data cannot, however, distinguish quenching due to peptide binding in close proximity to the acrylodan from that due to conformational changes as a result of peptide binding to a more distant site. However, we have shown previously (17) that peptide binding does not induce the same conformational change as inhibitor binding, nor does it alter protease sensitivity of N355 (data not shown), arguing against global conformational changes. This, together with the data presented below (Table I), argue in favor of peptide binding in proximity to Cys^{117}.

Peptide Binding Is Sensitive to Modification of Histidine Residues—The third approach to defining the peptide-binding site derived from the observation that peptide binding was pH-sensitive (Fig. 6*A* and Ref. 17). Binding was inhibited above pH 7.2 and was stimulated at pH near 6.0. In addition, binding was sensitive to imidazole; the presence of 6 mM imidazole reduced peptide binding by half (Fig. 6*B*). Both observations suggested that histidine residues might be involved in peptide binding by GRP94. Diethyl pyrocarbonate (DEPC) *N*-carbethoxylates the imidazole ring of histidine in a highly specific manner under certain conditions (19, 20) and is therefore useful in defining the role of histidines. DEPC treatment of N34–355 (after cleavage of the His_6 tag) abolished the peptide-binding activity of the protein as effectively as the inhibitor radicicol, whereas the ethanol solvent alone had no inhibitory effect (Fig. 6*C*). Hydroxylamine (HA) treatment restored the activity of the DEPC-modified protein (Fig. 6*C*), confirming that only modified His residues and not other amino acids (20) were important for the change in activity.

His^{125} Is Important for Peptide Binding—The N34–355 protein has four His residues, at positions 125, 194, 200, and 353. Based on the model (Fig. 2*B*), His^{125} was deemed to be the histidine residue most likely to be involved in the peptide-binding site. We therefore mutated His^{125} to either Asp, altering the charge, or to Tyr, replacing the imidazole ring with a phenol ring. The mutated H125D protein had almost no peptide binding activity, and the H125Y protein - only partial activity (Fig. 7*A*). Because the binding reaction has an unusually slow off-rate (17) and therefore is not in equilibrium, Hill plots cannot be used to calculate the affinity, but the fractional occupancy plot can be used to estimate the association constants. The fractional occupancies calculated for the wild type and H125Y proteins are superimposable (Fig. 7*B*), showing no significant difference between the association constants of the wild type and H125Y proteins. Because the saturation level of H125Y is ~0.6 of that of wild type, this analysis suggests that the H125Y mutation affects the active fraction of the protein, rather than binding by the active fraction.

The loss of binding activity is not due to global misfolding of the mutant proteins. First, both were purified as soluble proteins and displayed chromatographic properties akin to the wild type protein. Second, both H125D and H125Y expressed the monoclonal 9G10 epitope (data not shown). Third, H125D retained its ability to bind the inhibitor radicicol and respond to it by altering its conformation, as shown by the native gel mobility test in Fig. 7*C*. The same test shows that approximately half of the H125Y mutant is found in the fast migrating conformation even in the absence of radicicol, supporting the conclusion that the H125Y mutation decreases the fraction of active protein. However, the population of this protein that shows correct mobility (~50%) does appear to be capable of radicicol binding-induced conformational change (Fig. 7*C*). The relative abundance of this population is in agreement with the peptide saturation level of H125Y (~0.6 of that of wild type, Fig. 7*A*). Therefore, tyrosine at position 125 of N34–355, although decreasing the proportion of active protein, does not preclude peptide binding *per se*. Because, in contrast to histidine and tyrosine, aspartic acid at position 125 abolishes peptide binding, we propose that the nature of residue 125 is critical for peptide binding, confirming a strong prediction of the structural model.

His^{125} Is in Physical Proximity to the Bound Peptide—Al-

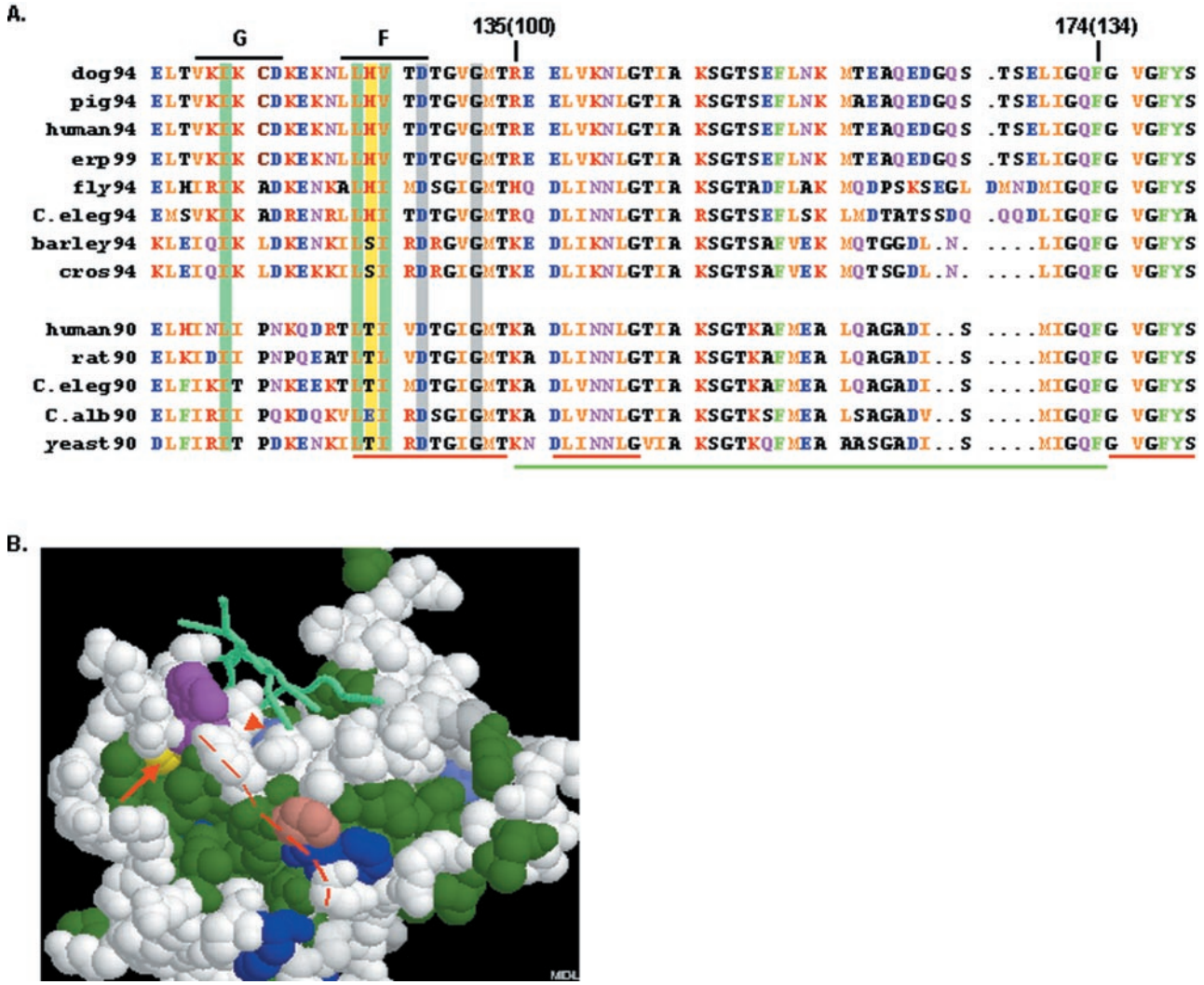

FIG. 4. **The predicted peptide-binding site is in proximity to a deep hydrophobic pocket and to the inhibitor-binding site.** *A*, multiple sequence alignment of parts of the N-terminal domains of GRP94 and HSP90. *Black lines* above the sequence, strands G and F (see *B*), containing Cys^{117} and His^{125}, respectively. *Red lines* below the sequence, inhibitor-binding pocket constituents (22, 26) within the partial sequence. *Green line*, 35 amino acids in HSP90 whose position is different between the geldanamycin-bound and free conformations. These are HSP90 residues 100–134 (*numbers in parentheses*), corresponding to residues 135–174 in GRP94. *Yellow highlight*, position 125; *gray highlights*, Asp^{128} and Gly^{132}, residues mutated in the RadR mutant; *green highlights*, Ile^{115}, Leu^{124}, and Val^{126}, residues contributing to the hydrophobic pocket. Other residues from the hydrophobic pocket are Leu^{80}, Ile^{84}, Leu^{240}, Ile^{243}, Val^{247}, Ile^{254}, Ile^{258}, Pro^{259}, and Val^{260}. Amino acids are *colored blue* for E or D; *red* for K, R, or H; *purple* for N or Q; *green* for F or Y; *brown* for C; *black* for A, G, P, S, and T; and *yellow* for I, L, M, and V. *B*, model of the hydrophobic pocket. A spacefill model showing the protein in the same view as in Fig. 2*B*, *left panel*. Peptides are shown in *light green*. *Dark green* residues, I, L, and V; *blue*, F; *purple*, T; *brown*, P; *yellow*, C; *light blue*, H. *Red arrow*, Cys^{117}; *red arrowhead*, His^{125}. *Red dashed line*, approximate location of the residues shown to cross-link to bis-ANS (28).

though the data above show that the environment of Cys^{117} changes upon peptide binding and that His^{125} modification either by DEPC or by a charge-altering mutation abolishes peptide binding, they can be explained in terms of transmission of conformational changes and thus do not formally show physical association. Therefore, we used the DEPC modification procedure in a peptide-protection experiment. The extent of DEPC modification was compared between a peptide-bound and peptide-free N34–355 (from which the His_6 tag was removed), reasoning that, if peptide is bound as modeled, it should protect His^{125} from modification. The proteins were analyzed by surface-enhanced laser desorption ionization/time-of-flight mass spectrometry (Table I). Each *N*-carbetoxylation adds 72 Da per His residue modified. The mass of N34–355 modified with DEPC increased by 289 Da compared with the unmodified protein, as expected from modification of all four His residues. That only His were modified was shown by the reversibility of the mass increase upon subsequent treatment with hydroxylamine (20). When N34–355 was saturated with peptide A prior to the modification with DEPC, the mass gain was 73 Da less than in the absence of peptide (Table I), as expected if one residue was protected from DEPC modification. Mass spectrometry of proteolytic fragments of DEPC-modified proteins confirms that the protected residue is His^{125} (data not shown). When the H125D mutant was used in the same manner, its mass increased by only 211–215 Da after modification with DEPC, whether peptide was present or not, as expected from a protein with only 3 His and unable to bind peptide (Table I). These modification experiments argue that of the four histidines, only His^{125} is involved in peptide binding, and it is physically associated with the peptide.

DISCUSSION

Many molecular chaperones recognize their substrates by binding to peptide sequences. Deciphering how GRP94 binds peptides is important not only for understanding how it acts as a chaperone, but also for understanding how it is able to stimulate peptide-specific T cell responses. The work presented

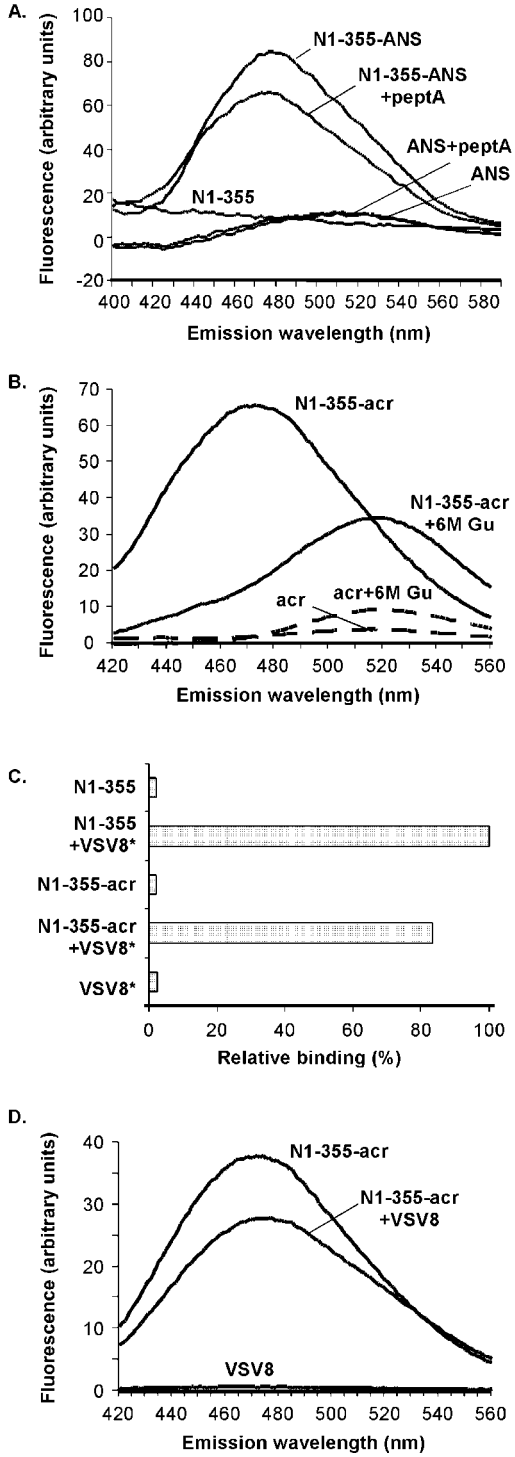

FIG. 5. **Peptide binding affects the environment of the hydrophobic pocket containing Cys^{117}.** *A*, peptide A binding affects the emission of N1–355-bound ANS. N1–355 was first reacted with ANS (N1–355-ANS) and then bound to saturating amount of peptide A (N1–355-ANS+peptA). Emission maximum of N1–355-ANS is 478 nm, indicating a highly hydrophobic environment. Addition of peptide A partially quenches the fluorescence of N1–355-ANS, but not that of free ANS. N1–355 itself does not fluoresce in the wavelength range shown. *B*, acrylodan binds covalently to the Cys within the predicted hydrophobic pocket. N1–355 and N34–355 were reacted with acrylodan overnight at 4 °C. A sample with identical amount of acrylodan without protein served as a control. Half of each sample was then supplemented with guanidine chloride to a final concentration of 6 M and another with equivalent volume of buffer. The emission maximum of N1–355-bound acrylodan under non-denaturing conditions was around 473 nm, indicating highly hydrophobic environment. In 6 M guanidine chloride, the emission maxima were around 522 nm for both N1–355-bound and free acrylodan, whereas the fluorescence intensity of the protein-bound acrylodan was significantly higher than that of the free dye, indicating covalent linkage. *C*, acrylodan conjugated N1–355 binds peptide to the same extent as unconjugated N1–355. Free or acrylodan-conjugated protein (3.6 μM) was reacted with 800 μM ^{125}I-VSV8 under saturating conditions and unbound peptide was removed using a spin column (17). Free ^{125}I-VSV8 was used to control for the efficiency of removal of the unbound peptide. N1–355 and N1–355-acr, free and acrylodan-conjugated protein respectively; N1–355+VSV8* and N1–355-acr+VSV8*, same proteins bound to ^{125}I-VSV8; VSV8*, free ^{125}I-VSV8 peptide. *D*, fluorescence of acrylodan covalently bound to N1–355 is affected by the addition of peptide. Fluorescence emission scans of acrylodan-conjugated N1–355 in the presence of either VSV8 (800 μM final concentration) or equivalent volume of buffer were taken at excitation wavelength 390 nm. VSV8 alone had no fluorescence in the measured wavelength range.

here provides an important part of the answer by locating the peptide-binding site. Together with our previous data (17), we show that the peptide-binding site of the chaperone GRP94 is located in a large groove in the N-terminal domain, opposite the nucleotide/geldanamycin/radicicol-binding site. This peptide-binding site was predicted by a computer docking algorithm, and the following experimental observations are consistent with the prediction: (*a*) residues 1–33 and 223–355 are dispensable for retention of bound peptide, if not for binding; (*b*) peptide binding is not hydrophobic in nature, consistent with the rather hydrophilic nature of the site; (*c*) Cys^{117}, located in a hydrophobic pocket, is affected by peptide binding, but can be modified covalently without inhibiting peptide binding; (*d*) alteration of the binding site for the inhibitor radicicol does not prevent peptide binding; (*e*) the nature of residue 125 is critical for peptide binding and His-125 is protected from modification with DEPC when peptide is bound; and (*f*) none of the other 3 histidines in N1–355 seems to be involved.

Substitution of Asp for His^{125} is sufficient to abolish the peptide binding activity of the protein. Although mutations that reduce or abolish peptide binding can lie outside the binding pocket and act by affecting protein conformation, we show physical association between His^{125} and peptide, because of the protection from modification by the small molecule DEPC when peptide is bound. Therefore, we propose that the curved β sheet in the N-terminal domain is a peptide-binding site of this chaperone, at least *in vitro*, and is not merely a regulatory site. A more extensive survey of amino acids by mutagenesis and other biochemical methods to map the extent of the binding site is in progress.

If the computer-generated model is correct also in predicting the mode of peptide association, then binding is along the axis of the groove with contacts along the entire length of the peptide, reminiscent of the interactions of peptides with the groove of MHC class I proteins. The saddle-like geometry of the proposed binding site would allow GRP94-binding peptides to "slide" along the axis of the groove, accounting for the observation that VSV8 binds with similar kinetics to VSV19, a peptide whose middle 8 amino acids are the VSV8 sequence. This aspect of the binding site would also explain the ability of GRP94 to bind peptides of different lengths, from 8-mers to 40-mers, with similar affinity (1, 15, 17).

While chaperones are generally thought to recognize hydrophobic peptides, as is true for HSP70s (31, 32), the features of peptides recognized by GRP94 seem different. The GRP94 groove identified here is lined with basic side chains (lysines and a histidine) and hydroxylic side chains (*e.g.* threonines), with only few hydrophobic side chains. The two binder peptides used in this work are also quite hydrophilic, their binding is sensitive to pH (Ref. 17 and this report) and is dissociated with high salt (17). Thus, binding of at least these peptides seems to be driven by polar and electrostatic interactions, not hydrophobic. This observation is also consistent with the nature of the

TABLE I

Protection of His^{125} from modification by peptide binding

Wild type N34–355 or the H125D mutant proteins were incubated with saturating concentration of peptide A (or buffer alone) and the complexes purified by spin column gel filtration. Proteins or protein-peptide complexes were then modified with DEPC (or the ethanol solvent alone) and adsorbed onto gold Ciphergen Protein chips. Masses of the treated proteins were determined by SELDI-TOF on a Ciphergen mass spectrometer calibrated with a standard set of proteins and peptides. The values given are for the single ionized peaks in each sample. They are from one experiment.

Protein and treatment	Observed molecular mass	Observed difference[a]	Expected difference[b]
	Da		
Wild type	37,742		
Wild type + DEPC	38,031	+289	+288 (4)
Wild type + DEPC + HA	37,758	+16	0
Wild type + peptide A +DEPC	37,955	+213	+216 (3)
H125D	37,767		
H125D + DEPC	37,978	+211	+216 (3)
H125D + DEPC + HA	37,737	−30	0
H125D + peptide A +DEPC	37,982	+215	+216 (3)

[a] The observed differences were calculated with respect to the unmodified protein (either wild type of H125D). The calculated molecular mass of wild type N34–355 is 37,781 Da, and that of the H125D mutant is 22 Da smaller. The differences obtained in two additional experiments were essentially identical.

[b] The expected differences were calculated based on modification of three or four His residues (indicated in *parenthesis*) and the addition of 72 Da to the mass of the protein by *N*-carbethoxy modification of each His.

His^{125} mutations that affect binding: replacing the imidazole ring with a Tyr side chain still allowed partial binding, and substituting with Asp completely inhibited binding. It will also be of interest to determine whether the H125D mutant is still capable to chaperone proteins.

The β strands that form the floor for the peptide-binding site separate it from the radicicol-binding pocket. The β sheet in the center of the domain appears to play a role in both activities of the N-terminal domain. This is clearly demonstrated here for strand F of this β sheet (Fig. 4*A*). It contains at least one residue, Asp^{128}, whose side chain is directed toward, and is important for binding to radicicol, as predicted from the homology with HSP90 (23) and shown directly in this work. The same strand F also houses His^{125}, whose central role in peptide binding is demonstrated here. Yet, despite their proximity, substitution of residues on the side of the strand that contacts the inhibitor does not significantly affect the contacts on the other side of the strand with bound peptide, and vice versa. We show that a radicicol-refractive mutant is able to bind peptide and that a mutant in peptide binding still responds normally to radicicol. Peptide binding can be inhibited by binding of radicicol, but the inhibitor has to occupy its binding site first (17). This suggests that binding of radicicol transmits a unidirectional change, either across the β sheet or more indirectly, so as to alter the peptide-binding groove.

The crystal structure of HSP90 has been solved both in the presence and absence of geldanamycin/radicicol/ATP, and the differences in structure help define the conformational change induced by occupation of the nucleotide site (22–23, 26, 33). The two forms differ in three helices and a loop, about 35 residues altogether, which mostly either enable or constrain the entrance to the nucleotide-binding pocket. The corresponding region in GRP94 is amino acids 135–174 (Fig. 4*A*). There is no obvious difference in the β sheet that would explain the inhibition of peptide binding by geldanamycin or radicicol. The observed inhibition, therefore, could be due to subtle changes or to more indirect transmission of conformational change from the 135–174 region to the opposite side of the molecule.

The identification of the peptide-binding site of GRP94 has direct relevance to all HSP90 proteins, because they have been reported to bind peptides, but none of their binding sites has yet been mapped. Scheibel *et al.* (34) showed that the N-terminal 210 amino acids of yeast HSP90 form a monomeric domain sufficient to bind peptides, in geldanamycin- and ATP-sensitive manner, much like the minimal GRP94 construct described here. Addition of the negatively charged domain to the N-terminal domain increases peptide-binding affinity without affecting specificity (35). Another similarity between yeast HSP90 and murine GRP94 is the apparent non-equilibrium nature of peptide binding (17, 35, and this report). Comparison of residues contributing to the saddle-like binding site shows that His^{125} is absent from all HSP90s, replaced by Thr in most HSP90 sequences. Because the HSP90 1–210 domain binds VSV8 less tightly than longer peptides (35), it is possible that the HSP90 N-terminal site is not as efficient in peptide binding as that of GRP94 or that its peptide specificity is different. An unresolved question for all HSP90 family members is the location of their client protein interaction site, and at least in the case of the kinase Akt this interaction is thought to be mediated by the middle domain of HSP90, rather than the N-terminal domain (37).

It is instructive to compare peptide binding by GRP94 with other peptide-binding sites. In HSP70 proteins, peptides also bind on top of a β sheet delineated by loops from the β sandwich domain (36, 38). The peptide makes contacts with three β strands and is perpendicular to them, and the binding groove has both hydrophobic and polar amino acids, but no charged residues (36, 38). In comparison, the GRP94 peptide groove is wider and is made up of mostly polar residues, and the peptide makes contacts more or less along the axis of three strands (strands G, F, and H). The interaction of GRP94 with peptide has several features in common with MHC proteins. In both MHC class I and class II the association constants are low and the off-rates very slow. GRP94-peptide complexes are very stable, resistant even to SDS, like many MHC-peptide complexes (39). When complexed with the K^b class I protein, the same VSV8 peptide used in the current work lies at approximately a 45° across a three-strand β sheet, constrained between two α helices (8), a topology that is similar to the one we suggest for the GRP94 binding groove. Interestingly, just like strand F, which provides important contact residues also on the other face of the β sheet with the inhibitors geldanamycin or radicicol, the same three β strands in MHC class I that interact with peptide also provide important contacts on the other face of the sheet with the β_2m subunit of the protein (40). Depending on the MHC allele (41), mutations in β_2m can alter such contacts and affect peptide loading on the other face of the β sheet (42).

MHC-peptide complexes are designed to leave one face of the bound peptide solvent-accessible, available for subsequent contacts with a T cell receptor. In HSP70 proteins, on the other hand, the bound peptide is buried, locked in place by an α-helical domain acting as a reversible latch, whose motion is con-

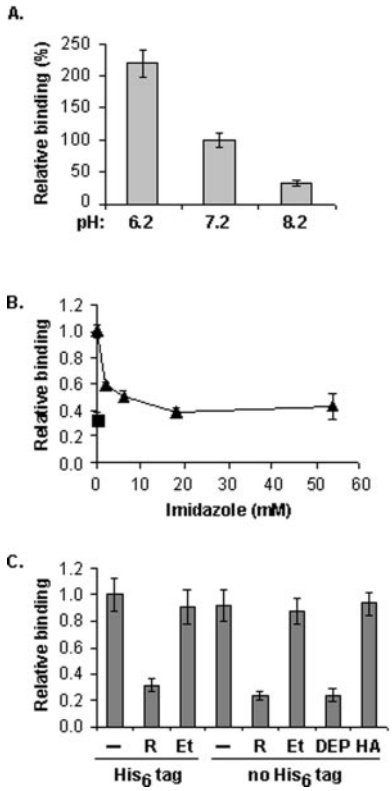

FIG. 6. **Peptide binding requires His residues.** *A*, peptide binding is pH-dependent. Binding of N1–355 to the peptide VSV8 was assessed at various pH values using the solution binding assay described previously (17). At pH 7.2, either Hepes or Pipes were used with equal results, and the average set to 100%. Hepes was used at pH 8.2, and Pipes was used at pH 6.2, with the average binding values normalized to that obtained at the standard pH of 7.2. *B*, peptide binding is sensitive to imidazole. Binding of N34–355 to peptide A was measured using the 96-well plate assay ("Experimental Procedures"). Imidazole was added to the indicated final concentrations, and the binding at each concentration normalized to that without imidazole. Peptide binding in the presence of radicicol is shown as a measure of the nonspecific binding. *Triangles*, binding in the absence on the inhibitor; *squares*, binding in the presence of radicicol. *C*, binding activity is abolished by DEPC modification. The His_6 tag of recombinant N355 was cleaved with factor Xa according to the manufacturer's instructions (Novagen) and the protein re-purified over a Ni-NTA column. The protein was treated with DEPC, as described under "Experimental Procedures," to modify histidines selectively. A portion of the modified protein was treated with 0.4 M hydroxylamine (HA), to reverse the DEPC effect. Modification with ethanol was used as a solvent control. Radicicol treatment was used to measure specific peptide binding. The untreated and modified proteins were allowed to bind to peptide A-coated plates (0.7 μg of protein per well) and binding was quantified by indirect reaction with 9G10 monoclonal antibody (Affinity Bioreagents) followed by horseradish peroxidase-goat anti-rat (Jackson Laboratories). Triplicate data points are from a representative experiment. DEPC decreased binding to the background level, whereas HA completely reversed the DEPC effect. Removal of the His_6 tag had no effect on either efficiency or specificity of binding. *R*, radicicol; *Et*, ethanol; *DEP*, treatment with DEPC; *HA*, treatment with DEPC followed by hydroxylamine.

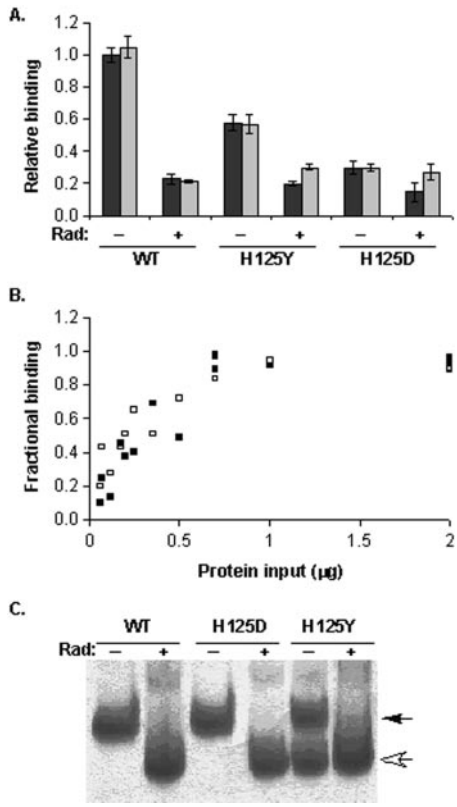

FIG. 7. **Site-directed mutagenesis demonstrates the importance of histidine 125 for peptide binding.** *A*, alteration of His^{125} affects N34–355 binding to peptide *A*, Wild type N34–355, H125Y, or H125D proteins were purified by metal chelate chromatography and their ability to bind peptide was tested in the plate assay (see "Experimental Procedures"). Inhibition by radicicol (300 μM) served as a specificity control (*Rad*). The binding was measured at two protein input levels (0.7 or 2 μg) based on the level of saturation binding for the WT protein. The data shown are averages and standard error of triplicate points in two experiments. *Black bars*, 0.7 μg of protein; *gray bars*, 2 μg of protein. *B*, fractional occupancy curves of wild type and H125Y. The amounts of peptide-bound protein, calculated as a fraction of the saturation binding level for each protein, is shown as a function of the input of protein. *Filled squares*, values from three independent dose-binding experiments for the wild type protein. *Empty squares*, values from three independent experiments for H125Y. *C*, the H125D mutant shows the expected structural change upon radicicol binding. H125D and H125Y were compared with WT protein using blue native gel electrophoresis. Each protein (10 μg) was treated with either 300 μM radicicol or with Me_2SO and then loaded on each of two adjacent gel lanes. After electrophoresis, the gel was stained with Coomassie Blue. Wild type and H125D proteins migrated predominantly as monomers and the characteristic radicicol-induced mobility shift was observed for both. Although H125Y protein also migrated as a monomer, it was present in two different conformations. Approximately half of H125Y showed increased mobility even in the absence of radicicol, whereas the other half showed both expected mobility and radicicol-induced conformational change. *Black arrow*, unbound protein; *white arrow*, radicicol-bound protein.

trolled by a nucleotide-induced conformational change (38). Our present data are not sufficient to decide whether GRP94-peptide complexes resemble one or the other models. It is possible that the second, acidic domain of GRP94 provides a locking mechanism for peptide, because it is needed for at least one activity of the N-terminal domain (25), and because it is involved a conformational change induced by binding of inhibitor to the N-terminal domain (17). The recently published structure of the N-terminal residues 48–316 of GRP94 (43) (residues 69–337 in the nomenclature used in that report) shows no obvious part acting to constrain the bound peptide from above. On the other hand, the acidic domain is unordered in the crystal structure and therefore can potentially regulate access to the peptide-binding pocket, in analogy to the long helix in HSP70 proteins (38). It is important to determine what structural feature "locks" the bound peptide, because on the one hand, peptides have been reported to have extremely high avidity to GRP94 (*e.g.* Refs. 1, 17, and 44), yet antigen presentation *in vivo* requires transfer of the GRP94-bound peptide to MHC proteins.

The peptide-binding site identified in this work may account for the T cell stimulatory activity of GRP94. Together with the data showing that the N-terminal GRP94 fragment can bind to antigen-presenting cells and activate T cells (45), our data indicate that immunologically relevant peptides bind at this

site and that the N1–355 fragment of GRP94 may suffice to account for peptide-specific activation of T cells. Because this site can be regulated by ligands that bind to the nucleotide site and to the hydrophobic pocket, binding of peptide to this site can be regulated by intracellular co-factors that are yet to be discovered.

Acknowledgments—We thank Steven Dimirsky for purification of recombinant proteins and all members of the lab for helpful discussions.

REFERENCES

1. Blachere, N. E., Li, Z., Chandawarkar, R. Y., Suto, R., Jaikaria, N. S., Basu, S., Udono, H., and Srivastava, P. K. (1997) *J. Exp. Med.* **186,** 1315–1322
2. Singh-Jasuja, H., Scherer, H. U., Hilf, N., Arnold-Schild, D., Rammensee, H. G., Toes, R. E., and Schild, H. (2000) *Eur. J. Immunol.* **30,** 2211–2215
3. Tamura, Y., Peng, P., Liu, K., Daou, M., and Srivastava, P. K. (1997) *Science* **278,** 117–120
4. Suto, R., and Srivastava, P. K. (1995) *Science* **269,** 1585–1588
5. Binder, R. J., Han, D. K., and Srivastava, P. K. (2000) *Nat. Immunol.* **1,** 151–155
6. Argon, Y., and Simen, B. B. (1999) *Semin. Cell Dev. Biol.* **10,** 495–505
7. Imarai, M., Goyarts, E. C., van Bleek, G. M., and Nathenson, S. G. (1995) *Cell. Immunol.* **160,** 33–42
8. Zhang, W., Young, A. C., Imarai, M., Nathenson, S. G., and Sacchettini, J. C. (1992) *Proc. Natl. Acad. Sci. U. S. A.* **89,** 8403–8407
9. Nieland, T. J., Tan, M. C., Monne-van Muijen, M., Koning, F., Kruisbeek, A. M., and van Bleek, G. M. (1996) *Proc. Natl. Acad. Sci. U. S. A.* **93,** 6135–6139
10. Wearsch, P. A., and Nicchitta, C. V. (1997) *J. Biol. Chem.* **272,** 5152–5156
11. Wearsch, P. A., Voglino, L., and Nicchitta, C. V. (1998) *Biochemistry* **37,** 5709–5719
12. Meng, S. D., Gao, T., Gao, G. F., and Tien, P. (2001) *Lancet* **357,** 528–529
13. Breloer, M., Marti, T., Fleischer, B., and von Bonin, A. (1998) *Eur. J. Immunol.* **28,** 1016–1021
14. Ishii, T., Udono, H., Yamano, T., Ohta, H., Uenaka, A., Ono, T., Hizuta, A., Tanaka, N., Srivastava, P. K., and Nakayama, E. (1999) *J. Immunol.* **162,** 1303–1309
15. Spee, P., and Neefjes, J. (1997) *Eur. J. Immunol.* **27,** 2441–2449
16. Baker-LePain, J. C., Reed, R. C., and Nicchitta, C. V. (2003) *Curr. Opin. Immunol.* **15,** 89–94
17. Vogen, S. M., Gidalevitz, T., Biswas, C., Simen, B. S., Stein, E., Gulmen, F., and Argon, Y. (2002) *J. Biol. Chem.* **277,** 40742–40750
18. Schagger, H., Cramer, W. A., and von Jagow, G. (1994) *Analyt. Biochem.* **217,** 220–230
19. Kalkum, M., Przybylski, M., and Glocker, M. O. (1998) *Bioconjug. Chem.* **9,** 226–235
20. Rai, S. S., and Wolff, J. (1998) *J. Biol. Chem.* **273,** 31131–31137
21. Robert, J., Menoret, A., Basu, S., Cohen, N., and Srivastava, P. R. (2001) *Eur. J. Immunol.* **31,** 186–195
22. Prodromou, C., Roe, S. M., O'Brien, R., Ladbury, J. E., Piper, P. W., and Pearl, L. H. (1997) *Cell* **90,** 65–75
23. Roe, S. M., Prodromou, C., O'Brien, R., Ladbury, J. E., Piper, P. W., and Pearl, L. H. (1999) *J. Med. Chem.* **42,** 260–266
24. Schneidman-Duhovny, D., Inbar, Y., Polak, V., Shatsky, M., Halperin, I., Benyamini, H., Barzilai, A., Dror, O., Haspel, N., Nussinov, R., and Wolfson, H. J. (2003) *Proteins* **52,** 107–112
25. Schulte, T. W., Akinaga, S., Murakata, T., Agatsuma, T., Sugimoto, S., Nakano, H., Lee, Y. S., Simen, B. B., Argon, Y., Felts, S., Toft, D. O., Neckers, L. M., and Sharma, S. V. (1999) *Mol. Endocrinol.* **13,** 1435–1448
26. Stebbins, C. E., Russo, A. A., Schneider, C., Rosen, N., Hartl, F. U., and Pavletich, N. P. (1997) *Cell* **89,** 239–250
27. Prodromou, C., Siligardi, G., O'Brien, R., Woolfson, D. N., Regan, L., Panaretou, B., Ladbury, J. E., Piper, P. W., and Pearl, L. H. (1999) *EMBO J.* **18,** 754–762
28. Wassenberg, J. J., Reed, R. C., and Nicchitta, C. V. (2000) *J. Biol. Chem.* **275,** 22806–22814
29. Slavik, J. (1982) *Biochim. Biophys. Acta* **694,** 1–25
30. Prendergast, F. G., Meyer, M., Carlson, G. L., Iida, S., and Potter, J. D. (1983) *J. Biol. Chem.* **258,** 7541–7544
31. Blond-Elguindi, S., Cwirla, S. E., Dower, W. J., Lipshutz, R. J., Sprang, S. R., Sambrook, J. F., and Gething, M. J. (1993) *Cell* **75,** 717–728
32. Gragerov, A., and Gottesman, M. E. (1994) *J. Mol. Biol.* **241,** 133–135
33. Prodromou, C., Roe, S. M., Piper, P. W., and Pearl, L. H. (1997) *Nat. Struct. Biol.* **4,** 477–482
34. Scheibel, T., Weikl, T., and Buchner, J. (1998) *Proc. Natl. Acad. Sci. U. S. A.* **95,** 1495–1499
35. Scheibel, T., Siegmund, H. I., Jaenicke, R., Ganz, P., Lilie, H., and Buchner, J. (1999) *Proc. Natl. Acad. Sci. U. S. A.* **96,** 1297–1302
36. Burkholder, W. F., Zhao, X., Zhu, X., Hendrickson, W. A., Gragerov, A., and Gottesman, M. E. (1996) *Proc. Natl. Acad. Sci. U. S. A.* **93,** 10632–10637
37. Fontana, J., Fulton, D., Chen, Y., Fairchild, T. A., McCabe, T. J., Fujita, N., Tsuruo, T., and Sessa, W. C. (2002) *Circ. Res.* **90,** 866–873
38. Zhu, X., Zhao, X., Burkholder, W. F., Gragerov, A., Ogata, C. M., Gottesman, M. E., and Hendrickson, W. A. (1996) *Science* **272,** 1606–1614
39. Collins, E. J., and Frelinger, J. A. (1998) *Immunol. Rev.* **163,** 151–160
40. Shields, M. J., Assefi, N., Hodgson, W., Kim, E. J., and Ribaudo, R. K. (1998) *J. Immunol.* **160,** 2297–2307
41. Smith, R. A., Myers, N. B., Robinson, M., Hansen, T. H., and Lee, D. R. (2002) *J. Immunol.* **169,** 3105–3111
42. Shields, M. J., Kubota, R., Hodgson, W., Jacobson, S., Biddison, W. E., and Ribaudo, R. K. (1998) *J. Biol. Chem.* **273,** 28010–28018
43. Soldano, K. L., Jivan, A., Nicchitta, C. V., and Gewirth, D. T. (2003) *J. Biol. Chem.*
44. Liu, C., Ewing, N., and DeFilippo, M. (2004) *Methods* **32,** 32–37
45. Baker-LePain, J. C., Sarzotti, M., Fields, T. A., Li, C. Y., and Nicchitta, C. V. (2002) *J. Exp. Med.* **196,** 1447–1459